Journal of Nuclear Medicine, published on April 12, 2019 as doi:10.2967/jnumed.118.220871

A Quantitative Evaluation of Joint Activity and Attenuation Reconstruction in TOF-PET/MR Brain Imaging

Ahmadreza Rezaei[1] (corresponding author), Georg Schramm[1],

Stefanie M.A. Willekens[1], Gaspar Delso[2], Koen Van Laere[1], Johan Nuyts[1]

[1] KU Leuven - University of Leuven, Department of Imaging and Pathology, Nuclear Medicine & Molecular imaging; Medical Imaging Research Center (MIRC), B-3000, Leuven, Belgium.
[2] MR Applications and Workflow, GE Healthcare, Waukesha, Wisconsin.

CORRESPONDENCE:

Ahmadreza Rezaei, Department of Nuclear Medicine and Molecular Imaging, KU Leuven, Herestraat 49 - box 7003, 3000 Leuven, Belgium. Phone: +32 (163) 49080, Fax: +32 (163) 43759, Email: ahmadreza.rezaei@uz.kuleuven.be

FINANCIAL SUPPORT:

This work was supported in part by the Research Foundation Flanders (FWO) project G.0275.14N. A Rezaei and S Willekens are supported by FWO postdoctoral projects 12T7118N and 12W1418N, respectively. G Schramm is supported by NIH under grant: NIH P41 EB017183.

SHORT TITLE:

Joint reconstruction: A Brain Study

KEYWORDS:

Quantitative Analysis, Attenuation Correction, Joint reconstruction, Time-of-Flight PET

WORD COUNT:

4904

ABSTRACT

Time of flight (TOF) positron emission tomography (PET) data provide an effective means for attenuation correction (AC) when no (or incomplete or inaccurate) attenuation information is available. Since magnetic resonance (MR) scanners provide little information on photon attenuation of different tissue types, AC in hybrid PET/MR scanners has always been challenging. In this contribution, we aim at validating the activity reconstructions of the maximum likelihood activity and attenuation reconstruction accelerated using ordered subsets (OSAA) algorithm on a patient brain dataset. We present a quantitative comparison of the joint reconstructions with the current clinical gold-standard ordered subsets expectation maximization (OSEM) reconstruction using computed tomography (CT) based AC in PET/CT, as well as the current state-of-the-art in PET/MR, i.e. zero time echo (ZTE) based AC. **Methods:** The TOF-PET emission data were initially used in a preprocessing stage to estimate crystal maps of efficiencies, timing offsets and timing resolutions. Applying these additional corrections during reconstructions, OSAA, ZTE-based and the vendor provided atlas-based attenuation correction techniques were analyzed and compared to CT-based AC. In our initial study, we used the CT-based estimate of the expected scatter, and later used the ZTE-based and OSAA attenuation estimates to compute the expected scatter contribution of the data during reconstructions. In all reconstructions, a maximum likelihood (ML) scaling of the single scatter simulation estimate to the emission data was used for scatter correction. The reconstruction results were analyzed in 86 segmented regions of interest (ROIs) of the Hammers' atlas. **Results:** Our quantitative analysis shows that in practice a tracer activity difference of + 0.5% (±2.1%) and + 0.1% (±2.3%) could be expected for the state-of-the-art ZTE-based and OSAA AC methods, respectively in PET/MR compared to the clinical gold-standard in PET/CT. **Conclusion:** Joint activity and attenuation estimation methods can provide an effective solution to the challenging AC problem for brain studies in hybrid TOF-PET/MR scanners. With an accurate TOF-based (timing offsets and timing resolutions) calibration, and similar to the results of the state-of-the-art method in PET/MR, regional errors of joint TOF-PET reconstructions are within a few percent.

INTRODUCTION

Correction of positron emission tomography (PET) data for photon attenuation is necessary for quantitative reconstruction of the tracer distribution. This is typically done by means of a well aligned and energy-adjusted computed tomography (CT) image. Since magnetic resonance (MR) images provide little information on the electron density (closely related to linear attenuation) of different tissue types, the problem of attenuation correction (AC) remains challenging in the current state-of-the-art PET/MR scanners. It was shown that when time of flight (TOF) information is available, the attenuation sinogram can be uniquely estimated from the emission data up to a global constant, which translates into a related shape and position dependent additive term in the attenuation reconstruction (*1*,*2*). This finding has renewed the interest on the topic of joint reconstructions of activity and attenuation from emission data, in TOF PET scanners (*3*–*5*) as well as in non-TOF PET scanners (*6*).

Among the methods that have been proposed to determine the global constant in joint estimation are those that incorporate a tissue intensity prior, which enforces reconstruction of certain tissue attenuation types or values. However, the application of a tissue intensity prior requires careful consideration as the prior should preferably:

- not hamper the implicit alignment of the joint activity and attenuation reconstructions,
- solve the missing scale using knowledge of a generic tissue type, and
- allow patient specific attenuation values.

Furthermore, a convex prior is preferred, to avoid the creation of (possibly additional) local maxima. Nevertheless it should be noted that the problem of joint activity and attenuation estimation from TOF PET data is not guaranteed to be jointly convex.

In order to introduce joint reconstruction methods into routine clinical practice, comprehensive validation studies on big patient datasets are necessary. With a focus on comparative studies on the brain, the joint reconstruction method was found to introduce more bias in the tracer activity reconstructions when compared to an atlas-based AC approach in a collection of ^{18}F-FDG brain scans (*3*). Contrary to this finding, the accuracy of a different class of joint estimation methods was analyzed on a population of patient brain scans in (*7*), where the authors report that the joint estimation images were comparable to the gold-standard

MLEM reconstructions with CT-based AC. However this required a plane-dependent scaling to the activity reconstructions. In both studies, the expected scatter estimate of the emission measurements is assumed to be known, and the studies do not tackle the “chicken or egg” problem of the expected scatter and attenuation estimate in joint reconstructions.

In this work, we propose to add a uni-modal intensity prior favoring expected soft-tissue attenuation values within an MR derived soft-tissue mask, similar to the prior proposed by Ahn et al (*4*). In the generation of the soft tissue mask, we exclude pixels close to the soft tissue boundaries, to ensure that the (implicit) alignment of these boundaries is produced by the joint reconstruction framework and not by the tissue segmentation. Since soft-tissue can be identified in most MR images with relative ease and the soft-tissue photon attenuation is roughly similar between patients, we propose to add only a uni-modal soft-tissue intensity prior. Because the attenuation and activity are determined up to a constant (*1*,*2*), imposing the correct attenuation value within a soft tissue region is enough to ensure a quantitative tracer distribution. Due to the convexity of this prior, it would not adversely affect convergence. Beyond the MR-based soft-tissue mask, the joint estimation algorithm is then free to estimate patient specific attenuation values of structures such as cortical bone, air cavities, implants, etc. Furthermore, we investigate the combined problem of the expected scatter and attenuation estimation. Avoiding the scatter correction at first we find a biased activity and attenuation pair that best explains the emission measurements. Following this, the expected scatter and attenuation estimates are refined progressively in an interleaved manner.

MATERIALS AND METHODS

Data Acquisition

Emission data from a total of 34 brain ^{18}F-FDG patient scans (collected between 2016-10-13 and 2017-06-15) in a dementia study at our institute were acquired using the GE SIGNA PET/MR scanner with a coincidence timing resolution of 390 ps (*8*). The local institutional review board approved this study and informed consent was obtained from all subjects. The ZTE data were acquired using a standard head coil (8-channel HR brain, GE Healthcare) and the following MR sequence: 3D radial acquisition, flip angle of 0.8, image volume of 110 x 110 x 116 with an isotropic voxel size of 2.4 mm^3, number of averages 4 with a bandwidth of 62.5 kHz, and a total acquisition time of 42 s (*9*). Prior to PET/MR acquisition, CT images were

obtained using the Siemens Biograph HiRez PET/CT scanner. Patients (weight: 76.9 ± 21.4 kg) were injected with 147.1 ± 20.3 MBq ^{18}F-FDG and scanned for 20 minutes roughly an hour post-injection (62:07 ± 14:46 mm:ss). The GE PET Reconstruction Toolbox (MP24) was used to preprocess the raw emission data, and to estimate the expected scatter contribution.

Preprocessing

A quantitative reconstruction of the tracer activity distribution of joint estimation methods requires accurate data corrections during reconstructions as well as a more accurate calibration of the scanner. As reported in (*10*–*12*), OSAA and OSEM converge to different solutions when the scanner calibrations or the scatter estimates suffer from inaccuracies. To mitigate inaccuracies due to crystal calibration effects, maps of crystal efficiencies (XE), crystal timing offsets (XTO) and crystal timing resolutions (XTR) were estimated from the emission data (*11*,*12*), assuming perfect knowledge of the attenuation and scatter corrections. During data collection the scanner was calibrated multiple times.

To estimate scatter, the vendor scatter estimation software was used to produce a scatter estimate, given a particular emission sinogram and attenuation map (based on CT, ZTE (*13*) or OSAA (*2*)). Then, an OSEM reconstruction was computed with joint estimation of a global scatter scale factor, as proposed by Salvo et al (*14*), and the scatter was scaled accordingly in the further processing.

To ensure optimal calibration for each individual study, the crystal maps were estimated from the patient emission scans themselves. A chronological view of the crystal maps is shown in Figure 1, which confirms that the scanner is stable between subsequent calibrations.

Studies

Two scenarios were realized for this study. In the first, joint reconstructions were compared to the gold-standard reconstructions with the best practically obtainable estimate of the expected scatter contribution in the emission data, i.e. the CT-based estimate of the scatter. In addition to this comparison, activity reconstructions using an atlas-based (vendor provided) and a ZTE-based attenuation (*13*,*15*) correction were also compared to the gold-standard reconstruction. The ZTE-based attenuation was computed with a research tool provided by GE (v.1.6.2), which is featured in the MP 26 software release of the SIGNA PET/MR. The second scenario involves the comparison of activity reconstructions when the expected

scatter was estimated using the corresponding ZTE-based and joint attenuation images. In the latter case, 3 global iterations, each consisting of a joint reconstruction and a scatter estimation, were applied. A schematic of the studies is depicted in Supplemental Figure 1.

Standard Reconstructions

OSEM activity reconstructions were obtained with 3 iterations and 28 subsets using the CT-based attenuation (after a rigid alignment, using an in-house registration package, obtained by maximizing the normalized mutual information of the CT images to the Dixon in-phase MR sequence images), the ZTE-based and the vendor provided atlas-based attenuation correction factors (ACF). The activity images were reconstructed without point spread function modelling in a 210 × 210 pixel grid of 3.125 mm width transaxially and 89 planes of 2.78 mm width axially. The hardware (i.e. bed and head-coil) attenuation images were read from a template and combined with each of the attenuation images. The OSEM reconstructions using CT-based ACFs were used as the gold-standard.

Joint Reconstructions

The ordered subsets activity and attenuation (OSAA) reconstruction algorithm (*2*) was used to quantitatively reconstruct the tracer activity distribution and the attenuation image. An MR-based soft-tissue favoring intensity prior (restricted to a soft-tissue mask) was incorporated in OSAA. The algorithm was initialized with a uniform disk of activity and uniform tissue attenuation in the patient support. This patient body contour was obtained by thresholding the in-phase MR sequence images and the PET emission measurements. The known hardware attenuation images were manually added during reconstruction. To avoid attenuation build-up in the background (i.e. outside the regions with non-negligible tracer uptake), a trick was used to encourage zero attenuation along lines of zero activity. For such lines, the measured and forward projected count are both set to a predefined small positive value, such that the attenuation is (gently) driven to zero in each attenuation update step (*16*). OSAA reconstructions were then obtained after 3 iterations and 28 subsets (updating the activity once and the attenuation twice in each iteration) using an in-house implementation of the projector. Following the OSAA activity and attenuation estimation, the activity image is discarded. “Standard” activity images are then produced by standard OSEM reconstructions (3 iterations of 28 subsets) using the OSAA attenuation estimate to minimize possible differences in the

convergence level compared to the gold-standard reconstruction. In the following, we will still use the term "OSAA activity images" to denote these "standard" OSEM images obtained using the OSAA attenuation estimate.

MR Prior Design

A soft-tissue mask was generated by thresholding the ZTE MR-based attenuation estimate (*15*,*17*,*18*) to discard air and bone. The mask was then eroded (with a spherical structure with the voxels within a radius of 2 voxels from the central element set to 1) to limit the effects of the intensity prior close to soft-tissue boundaries. A Gaussian distribution with a mean expected soft-tissue attenuation of 0.099 cm^{-1} was used as our soft-tissue intensity prior, which results in the application of a quadratic penalty to the likelihood. Although the prior was constructed from the ZTE volume, we believe that a similar volume could be estimated from other MR sequences.

Image Analysis

The activity reconstructions (with no post-reconstruction smoothing) are compared and evaluated in 86 segmented regions of interest (ROIs) defined by the Hammers' atlas (*19*) and segmented using PMOD v.3.8 (PMOD technologies LCC, Zurich, Switzerland). In our comparative analysis, the mean difference between two activity reconstructions, X and Y, was computed in all the segmented regions of interest as:

$$d_{rel}(X,Y) = \frac{\sum_{j\in ROI} Y_j - \sum_{j\in ROI} X_j}{\sum_{j\in ROI} X_j} \qquad (1)$$

where *X* is considered the reference method. The mean and, in brackets, the standard deviation are reported throughout the text.

RESULTS

Preprocessing

Figure 1 shows the crystal map estimates in chronological order estimated in the preprocessing stage. The XTR seem to have a stable structure, however for acquisitions between 2017-01-10 and 2017-03-06, the time-stamps of some crystals were generated by a secondary and less-accurate timing mechanism, resulting in a poorer timing resolution for those crystals. This problem was eliminated by (the maintenance

prior to) the calibration of 2017-03-28. During the acquisitions between 2016-10-14 and 2018-10-28, the imaging protocol was to use a flexible mirror on the patient head-coil. Since this extra attenuation was not accounted for in the attenuation correction factors, that attenuation was partly modeled by assigning a poorer efficiency to the crystals closest to the mirror (dark region at the crystal map extremes). Apart from this and a slightly less sensitive unit (which was replaced before the 2016-10-25 acquisition), the XE maps also seem to be stable in our dataset. However, the XTO maps do not seem to be as stable as the other two crystal maps, it has a structure which seems to vary between time calibrations on the scanner (red arrows). Interestingly, there seems to be a strong influence from the less accurate crystal timings (acquisitions between 2017-01-10 and 2017-03-06) on the XTO maps.

In reconstructions where each of the crystal map corrections were omitted (see Supplemental Figures 2 and 3), we found that correction of XTO had the most noticeable effect on the joint activity and attenuation reconstructions. The crystal timing offset problem observed here had been caused by strong assumptions about the phantom positioning during calibration. This problem has recently been solved by making the vendor calibration software insensitive to changes of the exact position of the phantom in the MP 26 software release of the SIGNA PET/MR.

Qualitative Assessment

Figure 2 shows OSEM and OSAA activity reconstructions as well as the attenuation images used/estimated for a patient dataset for the first reconstruction scenario (i.e. scatter correction using the CT-based expected scatter estimate). Visual inspection of the activity reconstructions seems to show more bias for the atlas-based OSEM reconstruction compared to the ZTE-based (also reported in (*18*)) and OSAA reconstructions. Furthermore, close inspection of the CT and the atlas images reveals missing attenuation near highly attenuating dental implants which are better recovered in the OSAA attenuation reconstruction, and hence are probably better accounted for in the OSAA activity reconstruction. In the OSAA attenuation reconstruction, we observe that the ear canal and surrounding hard bone look remarkably similar to the CT-based attenuation image.

Figure 3 shows activity reconstructions when the scatter estimate is computed from the ZTE-based and OSAA attenuation estimates (second scenario). For OSAA, the initial reconstruction was obtained without

scatter. This activity reconstruction together with its corresponding attenuation image (not shown here) was used to simulate an expected scatter estimate. The joint reconstruction of activity and attenuation of OSAA was interleaved with the scatter simulation algorithm and iterated 3 times (the intermediate OSAA activity difference images are shown in Supplemental Figure 4). In the final reconstruction (Figure 3), visually there does not seem to be a significant difference between activity reconstructions where the ZTE-based or the OSAA attenuation estimates were used for the expected scatter computation compared to activity reconstruction with the CT-based expected scatter estimates (Figure 2).

Quantitative Assessment

Figure 4, Figure 5 and Figure 6 show box plots of relative differences of all the activity reconstructions in our studies for all patients, the 86 segmented ROIs, and a further classification of the ROIs into 10 different classes in our patient datasets, respectively. The subscript “scatter” is used to denote the results when the scatter estimate was computed using the ZTE-based and the OSAA as opposed to the CT-based AC. Figure 7, shows the box plots of averages over both ROIs and datasets. For the reconstructions that used the CT-based scatter estimate, all three activity reconstructions, i.e. with the (vendor provided) atlas-based, ZTE-based and OSAA AC, achieved a reasonably low bias of + 0.4 %, + 0.2 % and + 0.6 %, respectively. However, the methods had varying accuracy levels over all ROIs with a standard deviation from the mean of 2.7 %, 0.8 % and 1.6 %, respectively. This was also reflected in the range of ROI differences, i.e. 50.8 % [-33.2, +17.6], 19.1 % [-12.6, +6.5] and 19.6 % [-8.7, +10.9], for the three studies respectively.

When the ZTE-based and OSAA attenuation estimates were used for the expected scatter estimation in addition to attenuation correction, a similar behavior was observed between the reconstructions. The relative difference (over all ROIs and datasets) in the estimated activity distribution produced a bias of + 0.5 % and + 0.1 % with a standard deviation of 2.1 % and 2.3 % for the ZTE-based and OSAA attenuation correction reconstructions. Both activity reconstructions had a similar range of ROI differences of 21.2 % [-13.5, 7.7] and 21.4 % [-13.8, +7.6], respectively.

Error! Reference source not found. shows a histogram of the relative ROI differences of all the regions and all datasets. As discussed above, the two cases that could be used in clinical practice when no CT is

available (ZTE-based and OSAA attenuation corrections and expected scatter estimation), seem to perform similarly.

DISCUSSION

The AC problem in hybrid PET/MR scanners is more challenging compared to hybrid PET/CT scanners. Since TOF measurements in PET provide information on the attenuation, this added information can be used to mitigate some of the related problems. With an accurate estimate of the expected amount of scatter in the emission measurements, joint reconstruction methods can only provide a scaled reconstruction of the tracer activity distribution. Hence extra constraining is required for a quantitatively accurate reconstruction of the activity distribution. The most intuitive approach is to constrain the reconstructed attenuation, as was also done in this work.

The simultaneous activity and attenuation (OSAA) reconstruction algorithm was incorporated with an intensity prior which favored expected soft-tissue attenuation values in an MR-determined tissue mask. The uni-modal soft-tissue intensity prior (a mean of 0.099 cm^{-1}) was enough to correct for the additional degree of freedom (a single scale) in joint reconstructions. The soft-tissue class was selected as the tissue prior of choice since it can be segmented from MR images with relative ease, but also because of its generic attenuation value across patient populations. During reconstructions, the algorithm was then free to assign any attenuation value to regions with bone, air cavity, dental implant, etc. The soft-tissue prior mask was eroded to avoid problems related to PET and MR data alignment, and although the ZTE sequence was used to determine this mask, we think that other MR sequences could also be used instead. It should however be noted that the “background trick” played a crucial role in limiting the buildup of attenuation in regions outside the activity distribution support. The reconstruction of attenuation outside the patient is not problematic in itself, even with these non-realistic attenuating structures in the background, the corresponding attenuation sinogram will still be accurate up to a scale factor. But since this background attenuation actually models part of the true object attenuation, that object attenuation must be decreased accordingly to obtain the correct scale factor. Consequently, with non-zero attenuation in the background, imposing tissue attenuation to soft tissue regions will result in an overestimation of the tracer activity

distribution. Therefore, the use of prior knowledge on attenuation values in the object must be combined with a regularization that encourages background attenuation to be zero.

An essential requirement for quantitative joint reconstructions is the knowledge of (and hence correction for) the expected amount of scatter in the measured emission data. In this work, we investigated scenarios where “perfect” knowledge of the expected scatter (using CT-based scatter estimate) was available, and we compared the reconstructions to a scenario where this information was not available. With an interleaved updating of the OSAA joint reconstructions and the expected scatter estimate, we showed that accurate tracer activity distributions can be reconstructed. The results were comparable to the state-of-the-art ZTE-based AC in PET/MR.

We have previously observed that joint reconstruction methods converge to another solution than conventional reconstruction with CT-based attenuation if modelling errors are present (*10*–*12*). In a preprocessing stage, we computed crystal map corrections to the systems’ XTO and XTR as well as XE. We have observed before (*10*–*12*) that these corrections can influence the reconstructions to different extents. In our patient brain dataset, the additional correction for the XTO had the greatest impact on the accuracy of the OSAA activity and attenuation reconstructions (Supplemental Figures 2 and 3), which visually seemed to be stable between timing calibrations. In our implementation, we observed roughly a two-fold increase in the processing time in reconstructions with the additional estimation (and correction) for the XE, XTO and XTR maps.

This study was focused on the analysis of AC methods for TOF-PET brain scans. With a similar accuracy to the ZTE-based AC method, we believe that OSAA-based AC could be considered as a method of choice, especially when the ZTE MR sequence is not available or is subject to inaccuracies, e.g. due to metal implants. Our ongoing work is aimed at analyzing joint reconstructions of OSAA on whole-body patient scans for the TOF-PET/MR.

CONCLUSION

In this contribution we aimed at the quantitative analysis and validation of joint activity and attenuation reconstructions from TOF-PET emission data in brain imaging. Our study demonstrates that the joint activity

and attenuation reconstructions from TOF-PET provides accurate tracer distribution reconstructions, comparable to the state of the art in PET/MR, i.e. ZTE-based AC, as well as the current clinical gold-standard, i.e. CT-based AC. For OSAA, the expected scatter contribution of the data and the joint reconstructions were updated and refined in an interleaved manner. Contrary to previous findings, we find that with accurate data corrections and scanner calibrations, activity reconstructions can be obtained with close to zero bias and with up to a few percent standard deviations.

ACKNOWLEDGMENTS

This work was supported in part by the Research Foundation Flanders (FWO) project G.0275.14N, FWO postdoctoral project 12T7118N. G Schramm has been supported by NIH under grant: NIH P41 EB017183. The authors would like to thank Floris Jansen, Sangtae Ahn, Timothy Deller and Kristen Wangerin from GE Healthcare for their help and support. The authors would also like to thank Michel Koole and Nathalie Mertens from the department of Nuclear Medicine and Molecular Imaging, UZ Leuven for technical help.

KEY POINTS

Question: How does the quantitative accuracy of joint activity and attenuation reconstructions of brain compare to the state-of-the-art activity reconstructions using the ZTE-based AC in TOF-PET brain studies?

Pertinent Findings: Joint activity and attenuation reconstructions provide accurate tracer distribution reconstructions, comparable to the state of the art in PET/MR, i.e. ZTE-based AC, as well as the current clinical gold-standard, i.e. CT-based AC.

Implication For Patient Care: In PET/MR studies, in cases where the ZTE MR sequence is not available or is subject to inaccuracies, joint reconstruction methods could be considered as a the reconstruction method of choice.

CONFLICT OF INTEREST

G Delso is an employee of GE Healthcare, Cambridge, UK. A Rezaei, G Schramm, K Van Laere and J Nuyts have received travel grants from GE Healthcare for attending workshops. G Schramm and K Van

Laere have received travel grants for presenting PET/MR results at GE user meetings. KU Leuven received a research collaboration grant from GE Healthcare. No other potential conflicts of interest relevant to this article exist.

REFERENCES

1. Defrise M, Rezaei A, Nuyts J. Time-of-flight PET data determine the attenuation sinogram up to a constant. *Phys Med Biol*. 2012;57:885–99.

2. Rezaei A, Defrise M, Bal G, et al. Simultaneous reconstruction of activity and attenuation in time-of-flight PET. *IEEE Trans Med Imaging*. 2012;31:2224–33.

3. Mehranian A, Arabi H, Zaidi H. Quantitative analysis of MRI-guided attenuation correction techniques in time-of-flight brain PET/MRI. *NeuroImage*. 2016;130:123-133.

4. Ahn S, Cheng L, Shanbhag DD, et al. Joint estimation of activity and attenuation for PET using pragmatic MR-based prior: application to clinical TOF PET/MR whole-body data for FDG and non-FDG tracers. *Phys Med Biol*. 2018;63:045006.

5. Rezaei A, Deroose CM, Vahle T, Boada F, Nuyts J. Joint reconstruction of activity and attenuation in time-of-flight PET: a quantitative analysis. *J Nucl Med*. 2018;59:1630-1635.

6. Ladefoged CN, Law I, Anazodo U, et al. A multi-centre evaluation of eleven clinically feasible brain PET/MRI attenuation correction techniques using a large cohort of patients. *NeuroImage*. 2017;147:346-359.

7. Bal H, Panin VY, Platsch G, et al. Evaluation of MLACF based calculated attenuation brain PET imaging for FDG patient studies. *Phys Med Biol*. 2017;62:2542.

8. Grant AM, Deller TW, Khalighi MM, Maramraju SH, Delso G, Levin CS. NEMA NU 2-2012 performance studies for the SiPM-based ToF-PET component of the GE SIGNA PET/MR system. *Med Phys*. 2016;43:2334-2343.

9. Wiesinger F, Bylund M, Yang J, et al. Zero TE-based pseudo-CT image conversion in the head and its application in PET/MR attenuation correction and MR-guided radiation therapy planning. *Magn Reson Med*. 2018;80:1440-1451.

10. Nuyts J, Rezaei A, Defrise M. The validation problem of joint emission/transmission reconstruction from TOF-PET projections. *IEEE Trans Radiat Plasma Med Sci*. 2018;2:273-278.

11. Rezaei A, Schramm G, Laere KV, Nuyts J. Data driven time alignment for TOF-PET. In: 2017 IEEE Nuclear Science Symposium and Medical Imaging Conference (NSS/MIC). ; 2017:1-3.

12. Rezaei A, Schramm G, Laere KV, Nuyts J. Estimation of crystal timings in TOF-PET. In: 2018 IEEE Nuclear Science Symposium and Medical Imaging Conference (NSS/MIC). ; 2018. In press.

13. Delso G, Kemp B, Kaushik S, Wiesinger F, Sekine T. Improving PET/MR brain quantitation with template-enhanced ZTE. *NeuroImage*. 2018;181:403-413.

14. Salvo K, Panin VY, Rothfuss H, Defrise M. ML estimation of the scatter scaling in TOF PET. In: 2015 Fully Three-Dimensional Image Reconstruction in Radiology and Nuclear Medicine Proceedings. ; 2015.

15. Sekine T, Voert EEGW ter, Warnock G, et al. Clinical evaluation of zero-echo-time attenuation correction for brain 18F-FDG PET/MRI: comparison with atlas attenuation correction. *J Nucl Med*. 2016;57:1927-1932.

16. Nuyts J, Dupont P, Stroobants S, Benninck R, Mortelmans L, Suetens P. Simultaneous maximum a posteriori reconstruction of attenuation and activity distributions from emission sinograms. *IEEE Trans Med Imaging*. 1999;18:393-403.

17. Wiesinger F, Sacolick LI, Menini A, et al. Zero TEMR bone imaging in the head. *Magn Reson Med*. 2016;75:107-114.

18. Schramm G, Koole M, Willekens SMA, et al. Regional accuracy of ZTE-based attenuation correction in static and dynamic brain PET/MR. *ArXiv Phys*. 2018.

19. Hammers A, Allom R, Koepp MJ, et al. Three-dimensional maximum probability atlas of the human brain, with particular reference to the temporal lobe. *Hum Brain Mapp*. 2003;19:224-247.

FIGURES

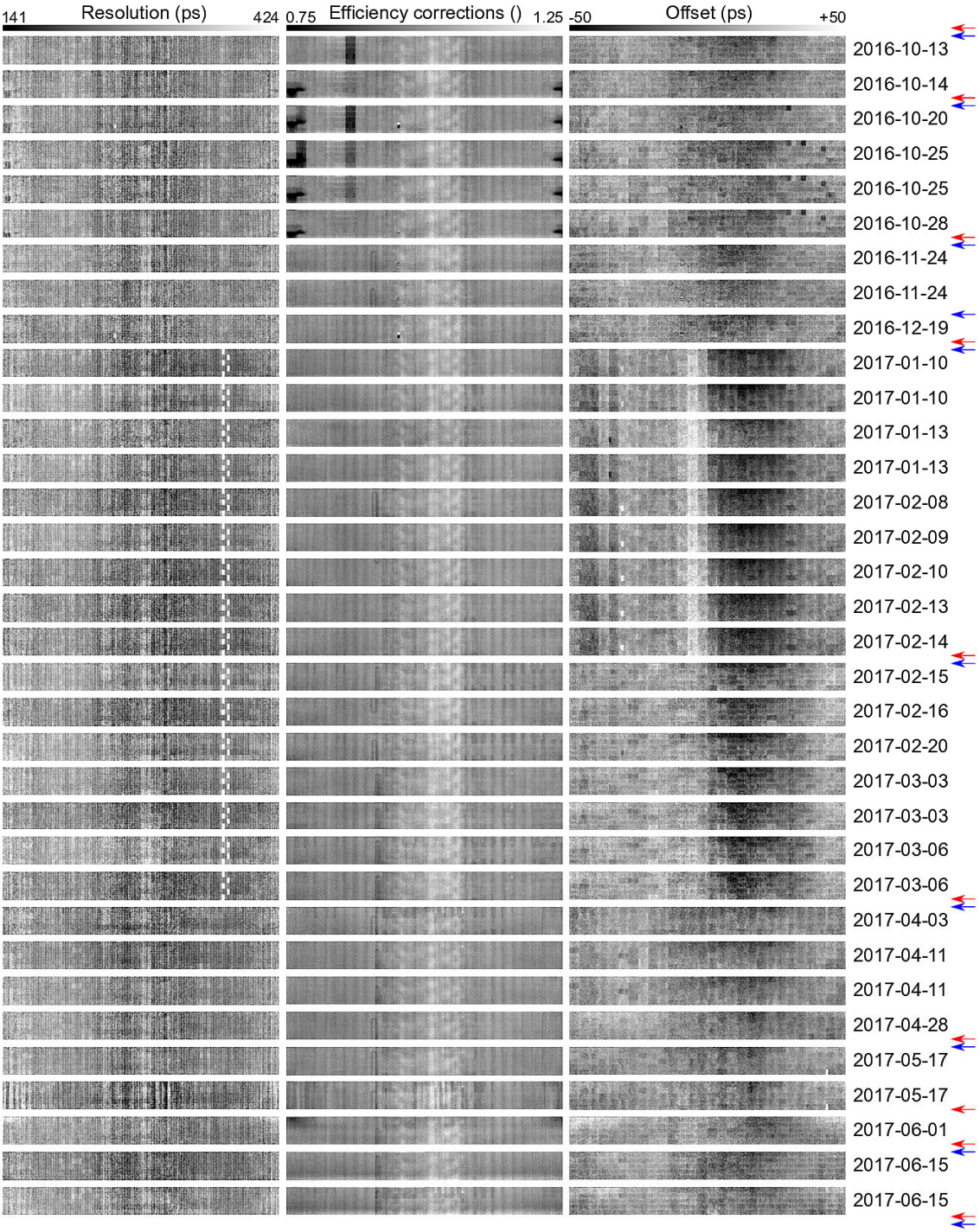

Figure 1 Crystal map of the timing resolutions (XTR, left), efficiencies (XE, center) and timing offsets (XTO, right) estimated from the emission data. The maps are shown in chronological (top to bottom) order. The red and blue arrows determine timing and efficiency calibrations on the PET/MR scanner, respectively.

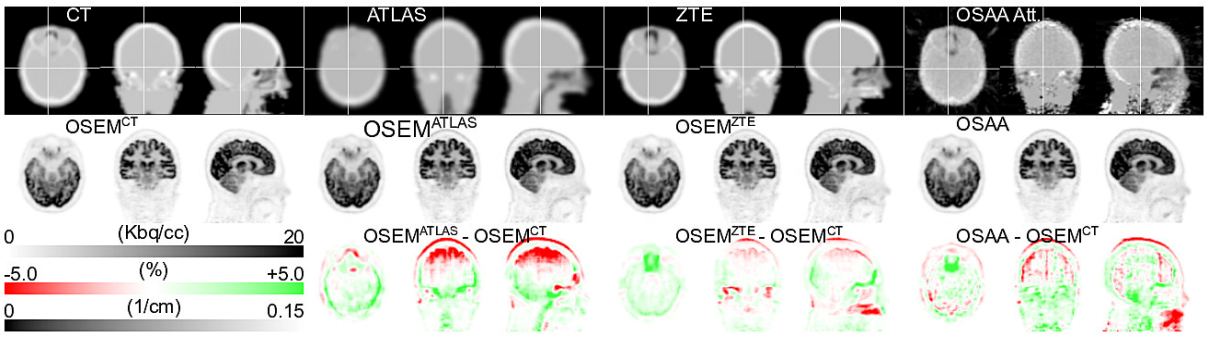

Figure 2 Transaxial, coronal and sagittal views of attenuation (top), activity (middle) and the activity difference (bottom) to the gold-standard reconstruction. In all these cases, the CT-based estimate of the expected scatter was used during reconstruction. Note that, the axial field of view of the CT was smaller than the PET/MR, hence the missing planes (neck region) were filled with the MR-based attenuation estimate.

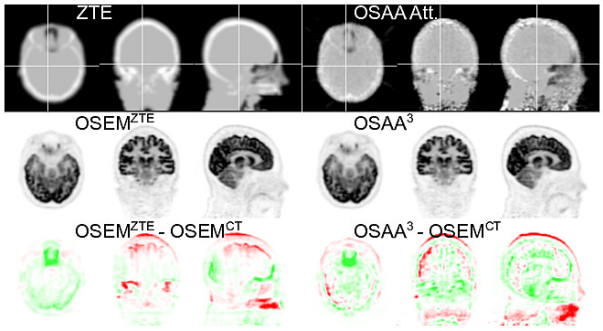

Figure 3 Transaxial, coronal and sagittal views of attenuation (top), activity (middle) and the activity difference (bottom) with the gold-standard reconstruction. In these cases, the ZTE-based and the OSAA attenuation estimates were used to estimate the expected scatter (the iteration number is indicated as a superscript for OSAA).

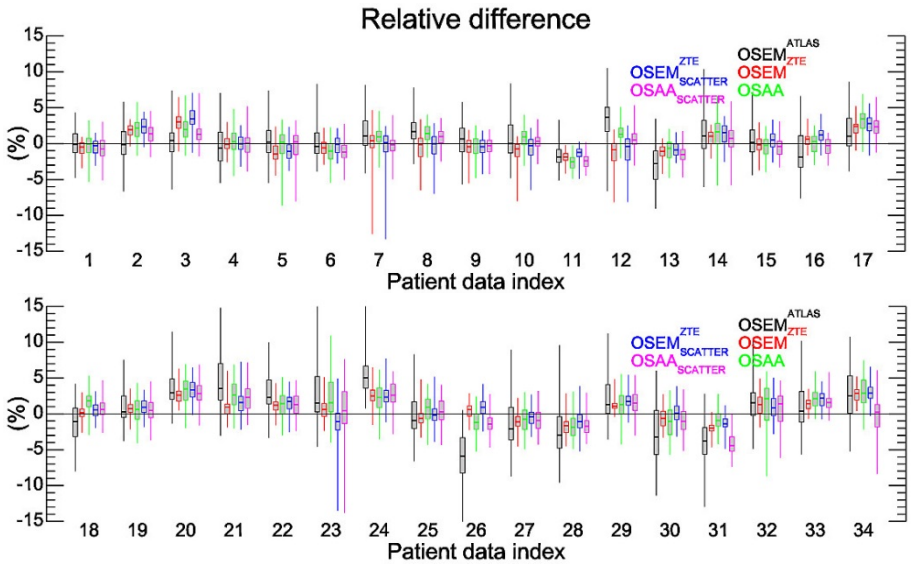

Figure 4 Box plot of the relative differences for the average 86 segments ROIs of the Hammers' atlas per patient.

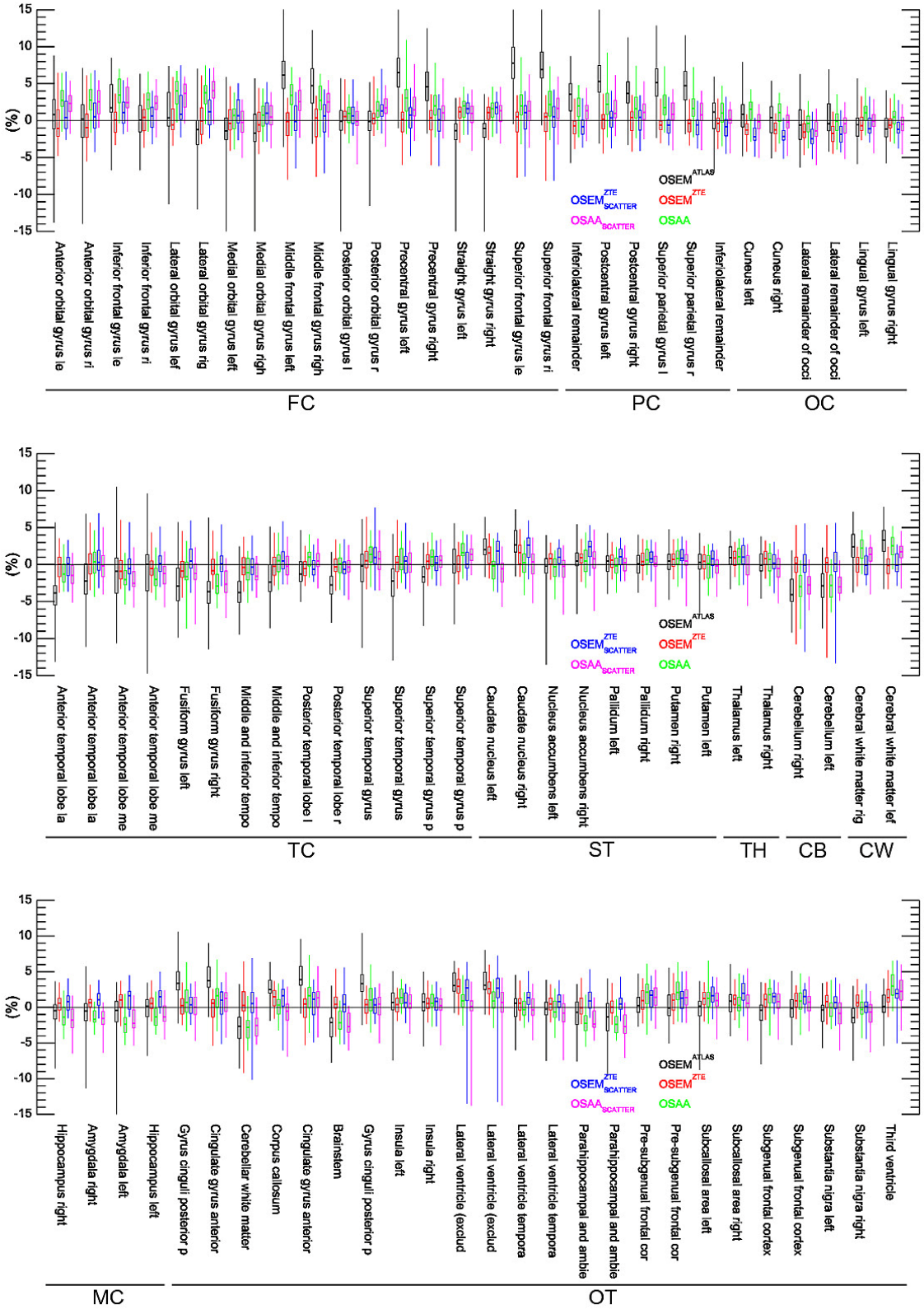

Figure 5 Box plot of the relative differences for the 86 segments ROIs of the Hammers' atlas averaged over all our patient datasets.

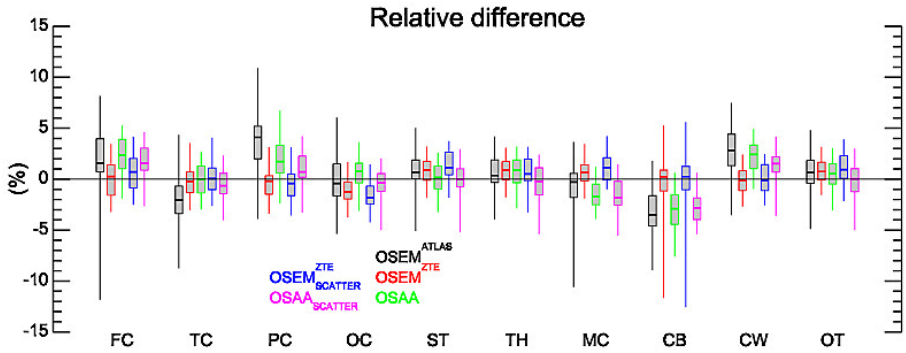

Figure 6 Box plot of the relative differences for 10 classified regions (FC: Frontal Cortex, TC: Temporal Cortex, PC: Parietal Cortex, OC: Occipital Cortex, ST: Striatum, TH: Thalamus, MC: Medial Temporal Cortex, CB: Cerebellum, CW: Cerebral White Matter, and OT: other) from the 86 ROI of the Hammers' atlas averaged over all our patient datasets.

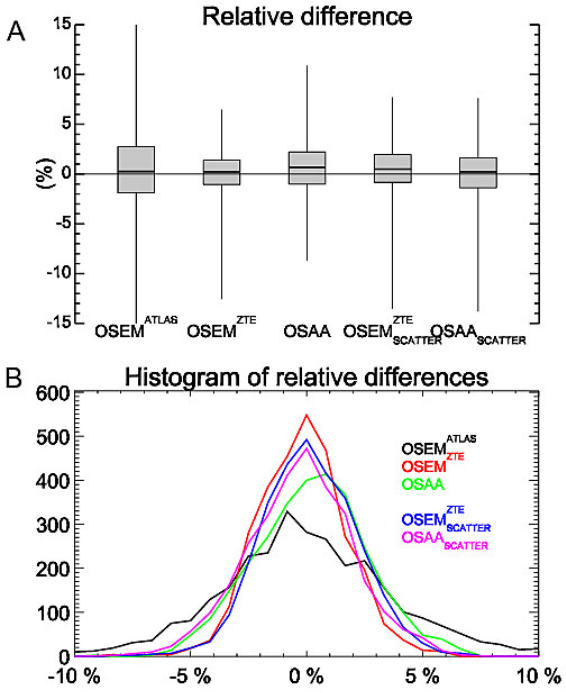

Figure 7 (a) Box plot of the relative differences averaged over all ROIs and all our patient datasets, and (b) Histogram of the relative differences compared to the gold-standard for all ROIs and all patient datasets.

A Quantitative Evaluation of Joint Activity and Attenuation Reconstruction in TOF-PET/MR Brain Imaging

Ahmadreza Rezaei[1] (corresponding author), Georg Schramm[1],

Stefanie M.A. Willekens[1], Gaspar Delso[2], Koen Van Laere[1], Johan Nuyts[1]

[1] KU Leuven - University of Leuven, Department of Imaging and Pathology, Nuclear Medicine & Molecular imaging; Medical Imaging Research Center (MIRC), B-3000, Leuven, Belgium.
[2] MR Applications and Workflow, GE Healthcare, Waukesha, Wisconsin.

FIGURES

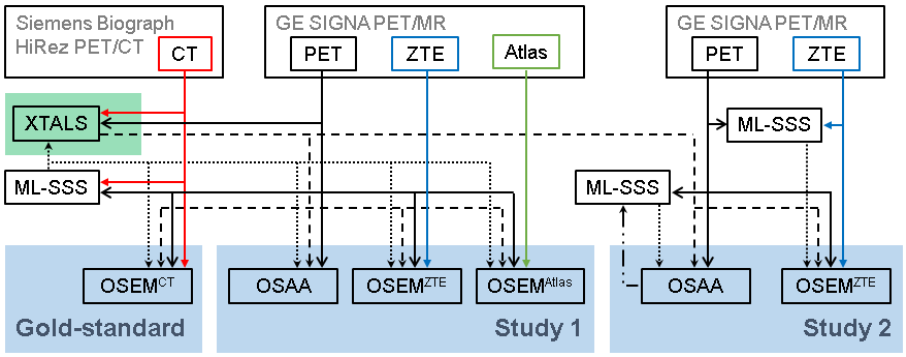

Supplemental Figure 1 Schematic of the studies. In study 1, joint reconstructions were compared to the gold-standard reconstructions with the best practically obtainable estimate of the expected scatter contribution in the emission data, i.e. the CT-based estimate of the scatter. In addition to this comparison, activity reconstructions using an atlas-based (vendor provided) and a ZTE-based attenuation correction were also compared to the gold-standard reconstruction. In study 2, the expected scatter was estimated using the corresponding ZTE-based and joint attenuation images. The Green block is the crystal-based pre-processing step which otherwise with an improved calibration would not have been needed.

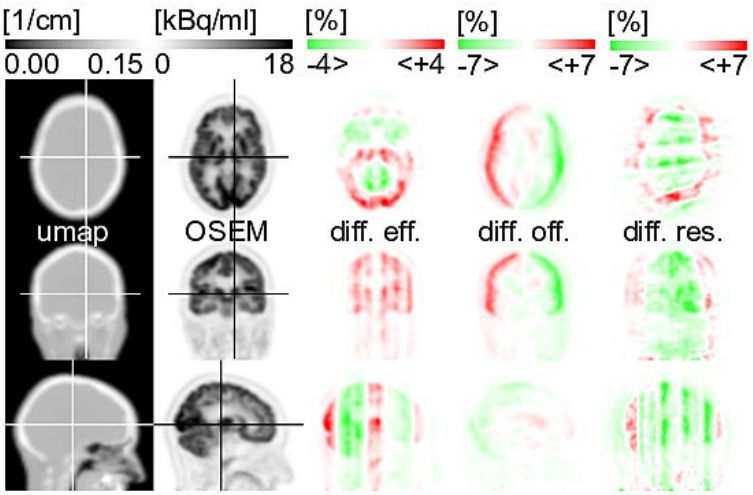

Supplemental Figure 2 Attenuation image (first column) and standard OSEM activity (second column) reconstruction with all the crystal map corrections of the 2017-02-10 scan shown in figure 4 applied to the GE SIGNA patient data. Difference images (columns 3-5) are after each of the crystal map corrections (efficiency correction factors, offsets and timing resolutions, respectively) are ignored. The OSEM activity reconstructions with all crystal-based corrections applied was used as reference when generating the difference images.

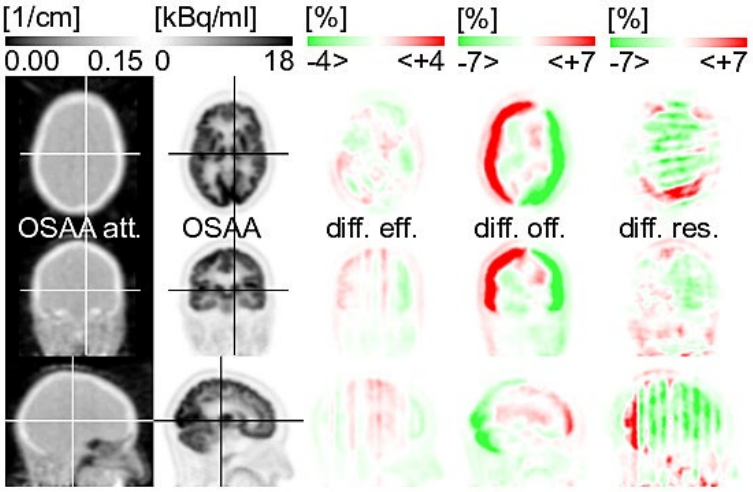

Supplementary Figure 3 OSAA Attenuation (first column) and activity (second column) reconstruction with all the crystal map corrections of the 2017-02-10 scan shown in figure 4 applied to the GE SIGNA patient data. Difference images (columns 3-5) are after each of the crystal map corrections (efficiency correction factors, offsets and timing resolutions, respectively) are ignored. OSAA activity reconstructions with all crystal-based corrections applied was used as reference when generating the difference images.

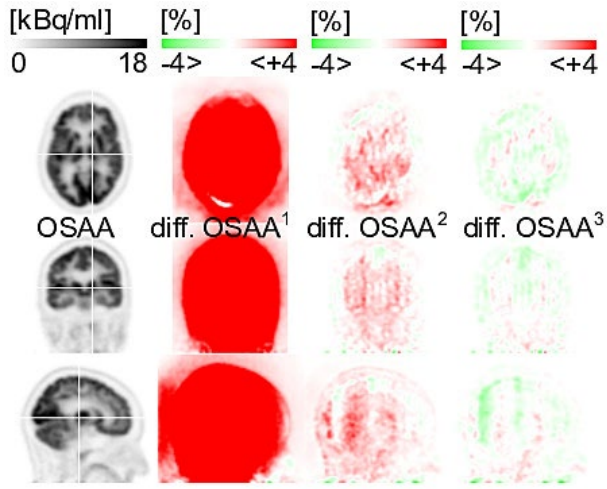

Supplemental Figure 4 Transaxial, coronal and sagittal views of OSAA activity reconstructions with the CT-based scatter estimate (first column) and difference images (columns 2-4) after each iteration (the iteration number is indicated as a superscript) when scatter was also estimated iteratively in an interleaved manner together with activity and attenuation reconstructions from the emission data. The OSAA activity reconstruction with the CT-based scatter estimate was used as reference when generating the difference images. In the first iteration, the reconstruction was without scatter correction (reflected by the high activity over-estimation (second column). This activity reconstruction together with its corresponding attenuation image (not shown here) were then used to simulate a scatter estimate. This interleaved scatter estimation and joint reconstruction scheme improved the scatter estimate from the previous iteration.